25th ABCM International Congress of Mechanical Engineering
October 20-25, 2019, Uberlândia, MG, Brazil

COB-2019-0448
EFFECTS OF LOADING SPAN ON CLEAVAGE FRACTURE TOUGHNESS OF PRECRACKED CHARPY-TYPE BEND SPECIMENS

Vitor Scarabeli Barbosa
Claudio Ruggieri
Polytechnic School of Engineering, University of São Paulo, Brazil
scarabeli@usp.br, claudio.ruggieri@usp.br

Abstract. *This work addresses an experimental investigation on the cleavage fracture behavior of typical structural steels using standard and non-standard PCVN configuration. The primary purpose of this study is to investigate the effects of loading span on cleavage fracture toughness measurements using non-standard bend specimens. Fracture toughness testing conducted on various PCVN geometries extracted from an A572 Grade 50 structural steel plate and an A515 Grade 65 pressure vessel steel plate provides the cleavage fracture resistance data in terms of the J-integral at cleavage instability, J_c. The experimental results show a potential effect of loading span on J_c-values which can help to mitigate the effects of constraint loss often observed in smaller fracture specimens. An exploratory application to determine the reference temperature, T_0, derived from the Master Curve methodology also provides additional support for using non-standard bend specimens in routine fracture applications.*

Keywords: *cleavage fracture, non-standard PCVN specimen, constraint effects, reference temperature, master curve*

1. INTRODUCTION

Current defect assessment procedures of large engineering structures employ macroscopic measurements of cleavage fracture toughness (such as the *J*-integral at cleavage instability, J_c, or the critical Crack Tip Opening Displacement, *CTOD*) derived from laboratory testing of conventional fracture specimens with deep, through cracks ($a/W \geq 0{,}5$). In particular, standard three-point bend specimens are routinely employed in toughness testing of ferritic steels in the ductile-to-brittle transition (DBT) region. These toughness measures must satisfy parametric limits on the crack-tip deformation relative to crack length, specimen thickness and remaining crack ligament such that high constraint conditions, similar to those of small-scale yielding (SSY), are maintained over microstructurally significant size scales at the crack-tip region. A recently developed procedure to characterize fracture toughness data over the DBT region, often known as the Master Curve approach (Wallin, 1991; McCabe et al., 2005) and standardized in the form of ASTM E1921-19 (2019), makes extensive use in practice of PCVN specimens to determine a reference temperature, T_0, and the associated median fracture toughness, $K_{Jc(med)}$, applicable to a wide range of structural ferritic steels. However, much previous research shows the potentially strong effects of specimen geometry and loading mode on J_c-values measured over the DBT region for ferritic materials. A case of considerable interest is the utilization of small fracture specimens to facilitate experimental measurements of fracture toughness data in commercial nuclear RPV surveillance programs. In particular, three-point bend testing of precracked Charpy (PCVN) specimens becomes necessary when severe limitations exist on material availability such as, for example, in nuclear irradiation embrittlement studies. However, the measuring capacity of small test specimens (as defined by the maximum applied values of J given by $J_{max} = (b\sigma_{ys})/M$ where M represents a nondimensional deformation limit, b denotes the uncracked ligament length and σ_{ys} defines the yield stress) for fracture toughness prior to constraint loss may be insufficient for moderate strength pressure vessel and structural steels. Once constraint loss occurs, the measured J_c-values increase markedly as the global plastic deformation interacting with the local crack front fields relaxes the levels of stress triaxiality. Motivated by these observations, this work addresses an experimental investigation on the cleavage fracture behavior of typical structural steels using standard and non-standard PCVN configuration. The primary purpose of this study is to investigate the effects of loading span on cleavage fracture toughness measurements using non-standard bend specimens. Fracture toughness testing conducted on various PCVN geometries extracted from an A572 Grade 50 structural steel plate and an A515 Grade 65 pressure vessel steel plate provides the cleavage fracture resistance data in terms of the *J*-integral at cleavage instability, J_c. The experimental results show a potential effect of loading span on J_c-values which can help to mitigate the effects of constraint loss often observed in smaller fracture specimens. An exploratory application to determine the reference temperature, T_0, derived from the Master Curve methodology (which defines the dependence of fracture toughness with temperature for the tested material) also provides additional support for using non-standard bend specimens in routine fracture applications.

2. DESCRIPTION OF CRACK-FRONT CONSTRAINT: THE *J-Q* APPROACH

The assessment of specimen geometry and loading mode (bending vs. tension) effects on fracture behavior for structural steels in the ductile-to-brittle (DBT) transition has received considerable attention in recent years. To evaluate the effects of specimen geometry in terms of loading span (with increased *S*/*W* ratios) on crack-tip constraint of bend specimens and its implications on the cleavage fracture toughness values measured in the DBT region, the present study adopts the *J-Q* methodology (1991; 1992) to characterize the crack front stress fields with increased specimen deformation. For further details, the interested reader is referred to the work of Dodds et al. (1993) and Nevalainen and Dodds (1995).

O'Dowd and Shih (OS) (1991; 1992) introduced an approximate two-parameter description for the elastic–plastic crack tip fields based upon a triaxiality parameter more applicable under large scale yielding (LSY) conditions for materials with elastic–plastic response described by a power hardening law given by $\epsilon/\epsilon_0 \propto (\sigma / \sigma_0)^n$. Here, n denotes the strain hardening exponent, σ_0 and ϵ_0 are the reference (yield) stress and strain, respectively. Guided by detailed numerical analyses employing a modified boundary layer (MBL) model, originally proposed by Rice (1967), OS defined the difference field relative to a high triaxiality reference stress state in terms of a hydrostatic parameter in the form of

$$Q \equiv \frac{\left(\sigma_{yy}\right)_{FB} - \left(\sigma_{yy}\right)_{SSY}}{\sigma_0} \tag{1}$$

where the difference field described in terms of the opening (Mode I) stresses, σ_{yy}, is conventionally evaluated at the normalized crack-tip distance $\bar{r} = r/(J/\sigma_0) = 2$, which represents a microstructurally significant distance ahead of crack tip related to the operative fracture mechanism. Here, it is readily understood that the dimensionless parameter Q defines the quantity by which σ_{ij} in fracture specimens, $(\sigma_{ij})_{FB}$, differ from the adopted high triaxiality reference SSY solution, $(\sigma_{ij})_{SSY}$. OS (1991; 1992), Dodds et al. (1991) and Cravero and Ruggieri (2005) have also shown that *Q* is relatively independent of *r* in the range $1 \leq \bar{r} \leq 5$. Construction of *J-Q* trajectories for structural components and fracture specimens then follows by evaluation of Eq. (1) at each stage of loading in the finite body. As will be shown in Section 4, construction of *J-Q* trajectories for the analyzed fracture specimens then follows by evaluation of Eq. (1) at each stage of loading in the finite body. The research code Fractus2D (2011) is employed to compute the *J-Q* curves for each fracture specimen shown in Section 4.

3. MATERIAL DESCRIPTION AND MECHANICAL PROPERTIES

The materials used in the fracture tests described next are a typical ASTM A515 Grade 65 pressure vessel steel with 294 MPa yield stress and 514 MPa tensile strength at room temperature (20 °C) and a high-strength-low alloy structural steel ASTM A572 Grade 50 with 376 MPa yield stress and 555 MPa tensile strength at room temperature, both steels supplied as a hot rolled plate. Table 1 lists the chemical compositions for the tested materials. It should be pointed out that both ferritic steels contain a less amount of C than the maximum values specified in ASTM A515-17 (2017) and ASTM A572-18 (2018) standards.

Table 1 - Chemical composition of steels ASTM A515 Grade 65 and ASTM A572 Grade 50 (% weight).

Steel (Grade)	C	Mn	Si	Nb	V	Ti	Cr	Ni	Mo
A515 (65)	0.26	0.67	0.26	0.001	0.003	0.002	0.03	0.01	0.01
A572 (50)	0.15	1.46	0.27	0.037	0.005	0.031	0.02	0.02	0.01

Mechanical tensile tests conducted on standard tensile specimens with 12.5 mm diameter extracted from the transverse plate direction provide the room temperature (T = 20 °C) stress–strain data. These test pieces were loaded in a 250 kN MTS servo-hydraulic universal testing machine with an axial extensometer to measure the specimen elongation according to ASTM E8/8M-16a (2016) requirements. Because fracture testing was conducted in the DBT region (see further details next), additional tensile tests were also conducted at T = - 20 °C on subsize test specimens with 6 mm diameter. Table 2 summarizes the tensile testing results for different test temperatures which evidence the high hardening behavior of the ASTM A515 Grade 65 steel with $\sigma_{uts}/\sigma_{ys} \approx 1.7 \sim 1.8$ and a moderate hardening behavior of the ASTM A572 Grade 50 steel with $\sigma_{uts}/\sigma_{ys} \approx 1.5$. Other mechanical properties for these materials include Young's modulus, E = 210 GPa and Poisson's ratio, ν = 0.3. Fig. 1(a) provides the engineering stress–strain curve for the ASTM A515 Grade 65 and ASTM A572 Grade 50 steel at room temperature and at T = -20 °C (average stress–strain response using data from three standard test specimens).

For reference, an improved estimate for the hardening exponent given by Annex F of API 579 (2016) provides the strain hardening exponents at the test temperatures (refer to Table 2) as n = 6.1 for T = 20 °C and n = 6.6 for T = -20 °C for the A516 steel and n = 8.0 at both temperatures for the A572 steel. It can be noted that these values are in accord with the uniaxial tensile behavior displayed in Fig. 1(a) in which the tensile response at T = -20 °C for the tested ASTM A516 Grade 65 steel shows a slightly higher hardening characteristic than at T = -20 °C for the tested ASTM A572 Grade 50 steel.

Table 2. Tensile properties of tested A515 Grade 65 and A572 Grade 50 steels, both at room temperature and at test temperature corresponding to the transverse plate direction (σ_{ys} and σ_{uts} denote the yield stress and tensile strength).

Steel (Grade)	T (°C)	σ_{ys} (MPa)	σ_{uts} (MPa)	σ_{ys}/σ_{uts}	n	ε_t (%)
A515 (65)	20	294	514	1.8	6.1	24
	-20	321	532	1.7	6.6	-
A572 (50)	20	376	555	1.5	8.0	14
	-20	407	601	1.5	8.0	15

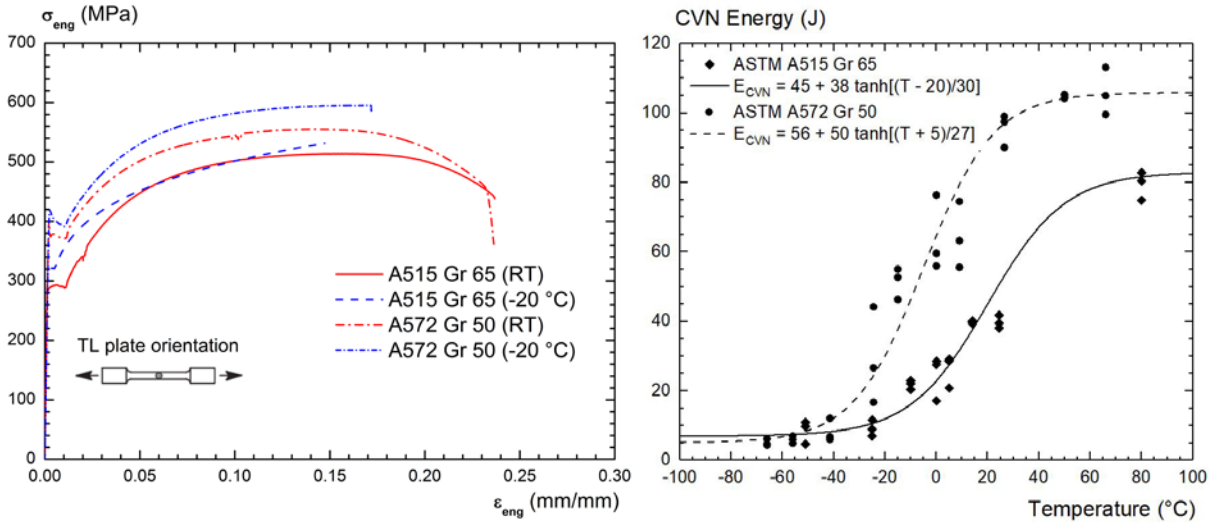

Fig. 1. (a) Engineering stress-strain curve (average stress-strain response using data from three test specimens) for the tested ASTM A515 Grade 65 and ASTM A572 Grade 50 steels at room temperature and at -20 °C. (b) Charpy-V impact energy (T-L orientation) versus temperature for the tested A515 Gr 65 and A572 Gr 50 steel.

A series of Charpy Tests were performed at different temperatures on standard V notch (CVN) impact specimens extracted in the TL plate orientation in order to aid for predicting a viable fracture toughness test temperature according to the ASTM E1921 (2019) recommendation. These sets of specimens were tested in a 406 J (300 ft•lbf) full-scale Tinius-Olsen pendulum machine, following the requirements of ASTM E23-18 (2018) standard. The specimens were tested at different temperatures whose temperatures ranges were defined between -66 and +80 °C. Fig. 1(b) shows the measured toughness-temperature properties for both steels in terms of conventional Charpy V-notch impact energy (T-L orientation). In this plot, the symbols represent the experimentally measured Charpy energy and the solid and dashed lines define a hyperbolic tangent curve fitting whose procedure, originally developed by Oldfield (1979), was based on the modified method proposed by Kirk et al. (2008) in the form

$$E_{CVN}^{\mathrm{A515}\ Gr65} = 45 + 38\tanh\left(\frac{T-20}{30}\right) \quad °\mathrm{C, J} \tag{2a}$$

$$E_{CVN}^{\mathrm{A572}\ Gr50} = 56 + 50\tanh\left(\frac{T+5}{27}\right) \quad °\mathrm{C, J} \tag{2b}$$

where E_{CVN} denotes the Charpy V-notch energy expressed in J and T is the test temperature in degrees Celsius. Using the above expressions, the Charpy transition temperatures corresponding to a 28 J energy yields approximately T_{CVN}^{28J} = -6 °C and T_{CVN}^{28J} = -22 °C for the A515 and A572 steels, respectively.

To investigate the effects of increased span on fracture toughness values measured in the DBT region, a series of toughness tests was carried out on standard and non-standard PCVN specimens in the T-L orientation. The fracture

mechanics tests include plane-sided, precracked Charpy (PCVN) specimen with a/W = 0.5, B = 10 mm, W = 10 mm and S = 4W and 8W. Here, a is the crack size, W denotes the specimen width, B represents the specimen thickness and S is the specimen span. Further, to provide a baseline reference temperature, T_0, for the tested materials, fracture toughness tests were also performed on conventional, plane-sided SE(B) specimens with a/W = 0.5, B = 2W wherein B = 30 mm for A515 and B = 25 mm for A572 steel, and S = 4W loaded under 3-point bending.

4. EFFECTS OF INCREASED SPAN ON *J-Q* TRAJECTORIES

This section provides key results of the constraint variations characterized in terms of *J-Q* trajectories to assess the potential effects of increased span on fracture behavior. To illustrate the effect of specimen span on the crack tip constraint of the tested bend configurations, Fig. 2 shows the *J-Q* curves measured from extensive plane-strain finite element analyses conducted for different strain hardening behavior. For further numerical details (e.g., finite element models, material model and solution procedures), and a comprehensive account of the framework needed to determine J and Q parameter, the interested reader is referred to the previous work of Barbosa and Ruggieri (2018). In all plots, Q is defined by Eq. (1) at the normalized distance ahead of crack tip given by $\bar{r} = r/(J/\sigma_0) = 2$ whereas J is normalized by ($b\sigma_{ys}$) with b denoting the remaining crack ligament (W-a) (notice that we plot $J/(b\sigma_{ys})$ vs. -Q to maintain positive scales). The finite element analyses consider material flow properties covering typical structural, pressure vessel and pipeline grade steels with E = 206 GPa and ν = 0.3: n = 5 and E/σ_{ys} = 800 (high hardening material), n = 10 and E/σ_{ys} = 500 (moderate hardening material) and n = 20 and E/σ_{ys} = 300 (low hardening material). The research code Fractus2D (2011) is employed to compute the *J-Q* trajectories for each fracture specimen. To aid in assessing the effect of increased span on the evolution of Q with J for the SE(B) specimens, the plot also includes the *J-Q* trajectory for a deeply-cracked, standard C(T) specimen with a/W = 0.6 and same hardening material derived from Cravero and Ruggieri (2005).

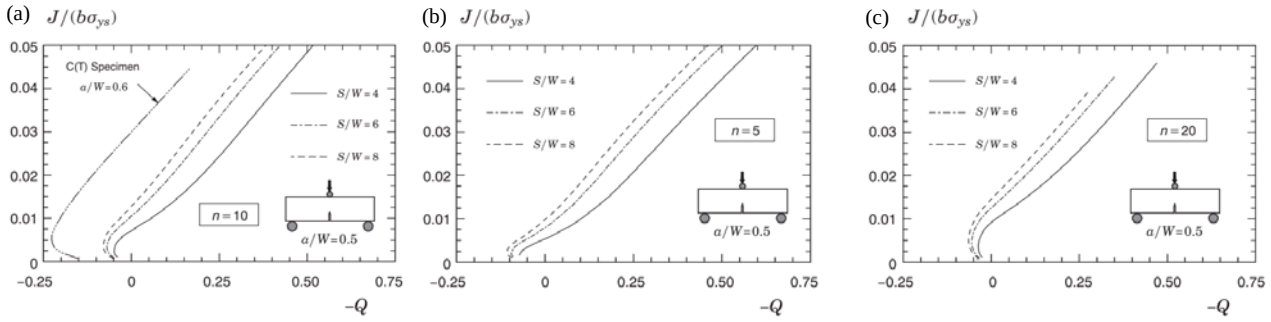

Fig. 2. *J*−*Q* trajectories for deep crack, 3P SE(B) specimens with varying S/W-ratios and a W = 0.5 material: (a) moderate hardening material; (b) high hardening material with n = 5; (c) low hardening material with n = 20.

Just to give an example, it can be observed that for a moderate strain hardening behavior, Fig. 2(a), as the load span increase, the J-Q trajectories is clearly shifted to the left. Crack-tip constraint, here characterized by parameter Q, is increased with increased specimen span as the *J-Q* curves shift entirely to the left toward to high constraint condition represented by C(T) specimen. Fig. 2(b) and 2(c) displays the effect of S/W -ratio on the evolution of Q with J for the deeply-cracked SE(B) specimen under 3P loading for the high hardening (n = 5) and low hardening (n = 20) materials. Not surprisingly, the general trends remain as crack-tip constraint is also increased with increased specimen span for any flow properties considered. This behavior suggests a potential mitigation effects of increased span and loading mode on constraint loss often observed in fracture testing of smaller bend specimens, such as the PCVN configuration, thereby increasing their measuring capacity.

5. FRACTURE TOUGHNESS DISTRIBUTIONS

Evaluation of cleavage fracture toughness values, here characterized in terms of J_c-values for the PCVN geometries and the deeply-cracked SE(B) specimen, follows from determining the plastic area under the load-CMOD curve and then using the estimation procedure given by Barbosa and Ruggieri (2018) from which the J_c -values are derived based on a new set of wide range of η-values applicable to standard and non-standard bend geometries. Figure 3 shows the (rank-ordered) cumulative probability distribution of the measured toughness values, J_c, for all tested fracture geometries. The cumulative probability, $F(J_c)$, is derived by simply ranking the J_c-values in ascending order and using the median rank position defined in terms of $F(J_{c,k}) = (k\text{-}0{,}3)/(N+0{,}4)$, where k denotes the rank number and N defines the total number of experimental toughness values (Mann et al., 1974). It is important to comment that this expression

can only be used, as such, for experimental data sets wherein all results correspond to failure. It can also be used with data sets where all results above a certain limit value has been censored e.g. due to non-failure or exceeding the measuring capacity limit, but in this case the data set size, N, must refer to the total data set including the censored data. The solid and open symbols in the plots indicate the experimental fracture toughness data for the specimens - observe that the open symbols in Fig. 3 represent the J_c -values for the PCVN configurations which exceeded the limit toughness value defined by $J_{lim} = (b_0\sigma_{ys})/M$ with the deformation limit, M, assigned a value of 30 as per ASTM E1921-19 (2019). The curves displayed in these plots describe the three-parameter Weibull distribution for J_c -values given by

$$F(J_c) = 1 - exp\left[-\left(\frac{J_c - J_{min}}{J_0 - J_{min}}\right)^{\alpha}\right] \tag{1}$$

in which α defines the Weibull modulus (which characterizes the scatter in test data) and is set to the value of 2, J_0 is the characteristic toughness (which corresponds to the 63.2% cumulative failure probability) and J_{min} denotes the threshold J-value corresponding to a K_{min} of 20 MPa√m as given by ASTM E1921-19 (2019). The trends are clear as the S/W-ratio affects rather strongly the fracture behavior for this specimen geometry. First, focus attention on the J_c-distribution for the plane-sided PCVN specimen with S/W = 4. Here, the toughness distribution for both materials is shifted to the right in comparison to the toughness distribution for the standard 1T SE(B) specimen thereby providing higher mean toughness values. Now examine the J_c-distributions for the PCVN specimen with S/W = 8. A different picture emerges as both toughness distributions are now shifted to the left and display decreased mean toughness values relative to the standard 1T SE(B) specimen. The implications of this apparent toughness changes for effects of specimen geometry in precracked Charpy (PCVN) configurations on predictions of the reference temperature, T_0, will be addressed in the next section. Table 3 provides the ML estimates of the characteristic toughness, $\hat{J}_0$, for all tested crack configurations determined according to ASTM E1921 (2019).

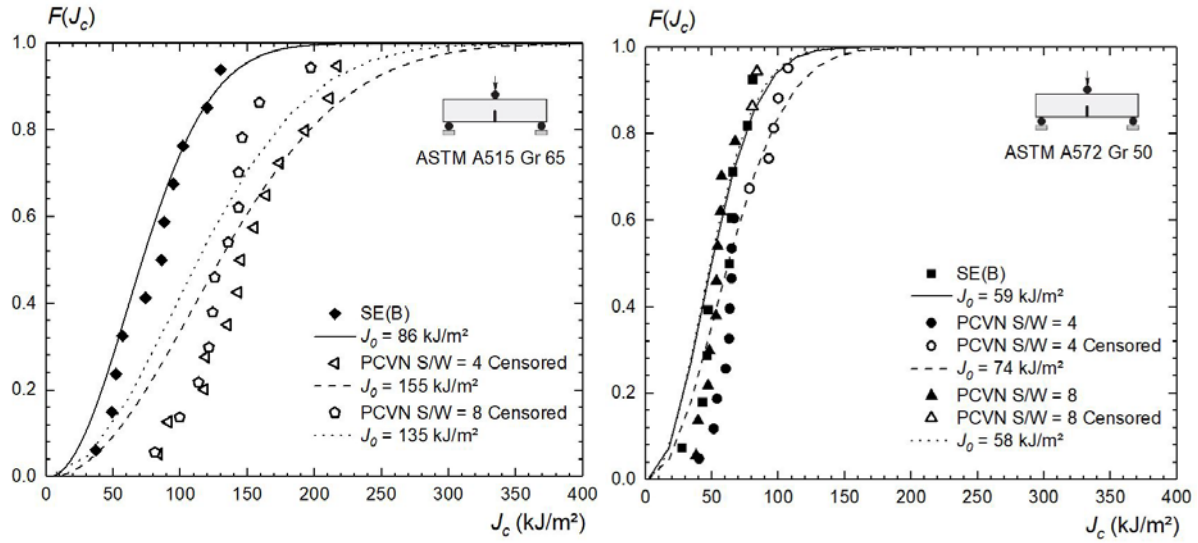

Fig. 3. Cumulative Weibull distribution of experimentally measured J_c-values from the (a) 515 and (b) A572 steels.

Table 3. Maximum likelihood estimates of the characteristic, $\hat{J}_0$, for the measured distributions of the J_c-values of each PCVN configuration, including the 1T-SE(B) standard configuration, and the corresponding estimates for T_0-values.

Material	Geometry	S/W	$\hat{J}_0$ (kJ/m²)	r/N	T_0 (°C)
ASTM A515 Gr 65	1T-SE(B)	4	86	11/11	-41
	PCVN	4	155	0/13	n.a.
	PCVN	8	135	0/12	n.a.
ASTM A572 Gr 50	1T-SE(B)	4	59	9/9	-26
	PCVN	4	74	9/14	-20
	PCVN	8	58	10/12	-11

As it can be observed, the effect of increased span on fracture toughness values seem to be more pronounced for a moderate strain hardening behavior. Reading from these results, a plausibly argument to explain this behavior can be made in terms of the higher crack tip constraint for the high hardening material in the early stages of loading once constraint effects are most pronounced for low-to-medium strength structural steels.

6. EVALUATION OF THE REFERENCE TEMPERATURE, T_0

Following the development provided in ASTM E1921-19 (2019), the reference temperatures for the tested materials are evaluated from the fracture toughness distributions for different PCVN configurations and the standard 1T SE(B) specimen. Table 3 compares the T_0-values obtained from the different PCVN configurations tested at $T = -20$ °C in which there is a clear and marked effects of increased span on the estimates for the reference temperature. To further illustrate the effect of specimen span on T_0 determined from using subsize specimens, Fig. 4 provides the variation of $K_{Jc\text{-}med}$ with temperature for selected PCVN configurations, including the standard 1T SE(B) specimen configuration. In these plots, the solid line defines the master curve of (corrected) median toughness, $K_{Jc\text{-}med}$, for 1T specimens whereas the dashed lines represent the 5% and 95% tolerance bounds for the maximum likelihood estimate of K_0. For the tested pressure vessel steel, the reference temperature yields the value of T_0 = -41 °C which is 21 degrees below the test temperature. Although the fracture toughness test temperature (T = -20 °C) is considerably higher than T_0-value, the master curve shown in Fig. 4(a) describes relatively well the dependence of fracture toughness with temperature once the proportion of data points below median curve (46%) is in accordance with the prediction of the ASTM standard. For this test temperature, the J_c-values obtained from the PCVN configurations are all censored and thus is not possible to estimate the reference temperature according to master curve approach.

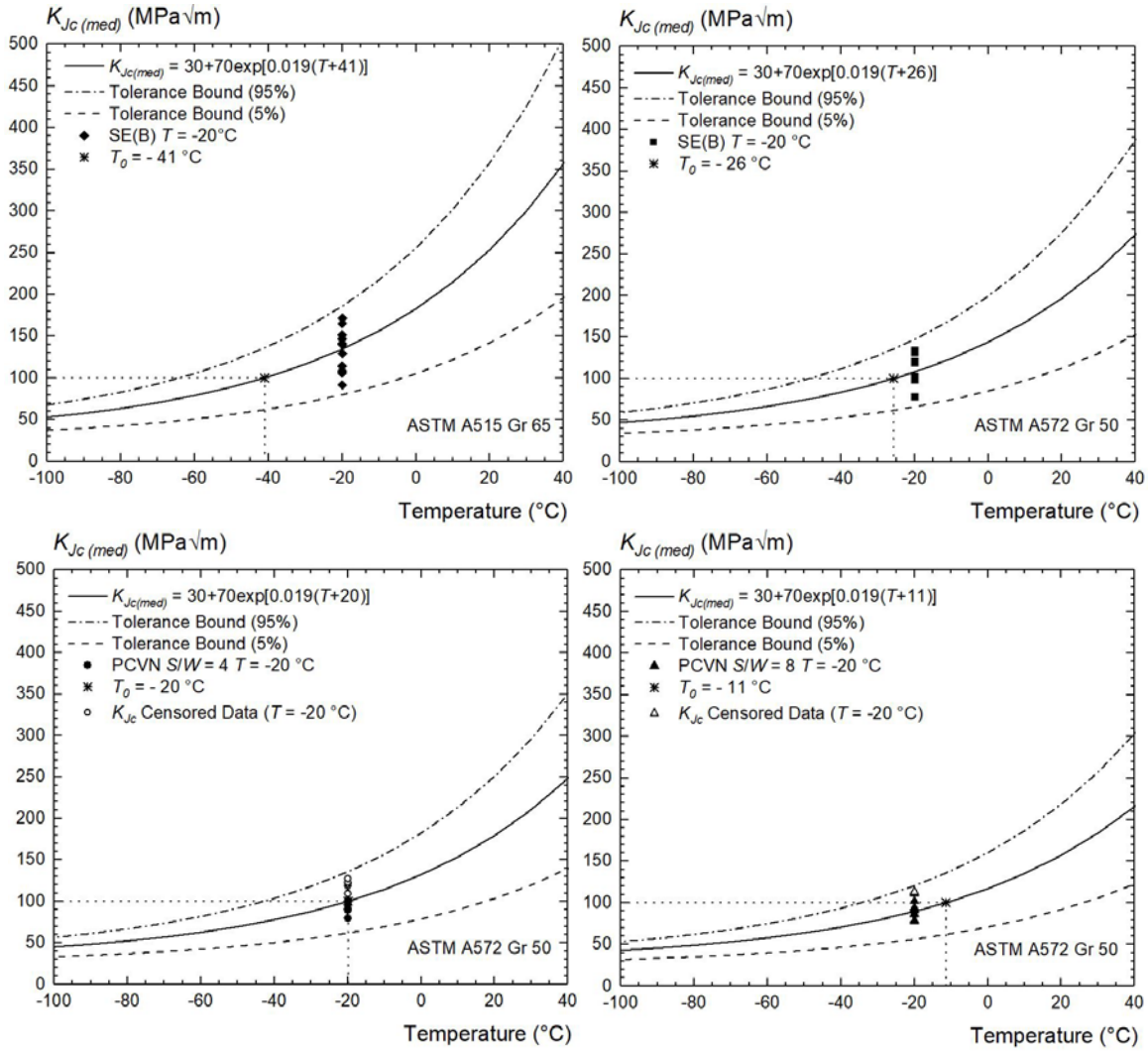

Fig. 4. Master curves for the tested A515 Gr 65 and A572 Gr 50 steels including 5% and 95% confidence bounds based on cleavage fracture toughness values measured from (a) A515 standard 1T SE(B) specimens with a/W = 0.5; (b) A572 standard 1T SE(B) specimens with a/W = 0.5; (c) PCVN specimens with S/W = 4; (d) PCVN specimens with S/W = 8.

Now, observe that the reference temperature for the tested ASTM A572 Grade 50 steel yields the value of $T_0 = -26$ °C which is about −6 degrees below the test temperature – this T_0-value is thus considered a "baseline" reference temperature in the present study. Since the test temperature of $T = -20$ °C is close to the T_0-value of −26 °C evaluated for the tested material, the master curve defined in Fig. 4(b) can thus be considered a good description of the variation of cleavage fracture toughness with temperature in the DBT region for the tested structural steel. Comparing the Figures 4(c) and 4(d) it can be observed that the increased specimen span appears to strongly limit the effects of constraint loss on measured fracture toughness for the PCVN configuration and on T_0. Moreover, also observe that the increased specimen span appears to produce a smaller number of invalid (censored) toughness values thereby resulting in more reliable estimates of K_0 and a better statistical description of the measured toughness distribution. Clearly, these latter results are strongly suggestive of the effectiveness of the non-standard PCVN geometry with increased span in mitigating the effects of constraint loss on T0-estimates often observed in standard PCVN configurations.

7. CONCLUSIONS

This study describes the results of a rather extensive fracture testing of an A515 Grade 65 pressure vessel steel plate and an ASTM A572 Grade 50 structural steel plate using non-standard PCVN specimens and an exploratory application to determine the reference temperature, T_0, and associated variation of cleavage fracture toughness with temperature for these materials. The fracture mechanics tests were performed on conventional, plane-sided SE(B) specimens with $a/W = 0.5$, $B = 2W$ wherein $B = 30$ mm for A515 and $B = 25$ mm for A572 steel, and $S = 4W$ loaded under 3-point bending; and (2) plane-sided, precracked Charpy (PCVN) specimen with $a/W = 0.5$, $B = 10$ mm, $W = 10$ mm and $S = 4W$ and $8W$. The experimental results show a potential effect of increased span on J_c-values which can help to mitigate the effects of constraint loss commonly observed in PCVN specimens. An exploratory application to determine the reference temperature derived from the Master Curve approach using fracture toughness values obtained from testing non-standard bend geometries, particularly the PCVN configuration with increased span, produces predictions for T_0 which are more conservative than the corresponding reference temperature derived from testing conventional, deeply cracked 1-T SE(B) specimens. Clearly, these results are strongly suggestive of the effectiveness of the non-standard PCVN geometry with increased span in mitigating the effects of constraint loss on T0-estimates often observed in standard PCVN configurations.

8. ACKNOWLEDGEMENTS

This investigation is supported by Fundação de Amparo à Pesquisa do Estado de São Paulo (FAPESP) through research grant 2016/26024-1. The first author (VSB) would like to acknowledge the financial support from Coordenação de Aperfeiçoamento de Pessoal de Nível Superior (CAPES). The work of CR is also supported by the Brazilian Council for Scientific and Technological Development (CNPq) through grant 306193/2013-2.

9. REFERENCES

API RP-579-1/ASME FFS-1, 2016. "Recommended Practice for Fitness-for-Service". *American Petroleum Institute*, New York, NY.

ASTM A515/A515M-17, 2017. "Standard Specification for Pressure Vessel Plates, Carbon Steel, for Intermediate- and Higher-Temperature Service". *ASTM International*, West Conshohocken, PA.

ASTM A572/A572M-18, 2018. "Standard Specification for High-Strength Low-Alloy Columbium-Vanadium Structural Steel". *ASTM International*, West Conshohocken, PA.

ASTM E8/E8M-16a, 2016. "Standard Test Methods for Tension Testing of Metallic Materials". *ASTM International*, West Conshohocken, PA.

ASTM E1921-19, 2019. "Standard Test Method for Determination of Reference Temperature, T0, for Ferritic Steels in the Transition Range, *ASTM International*, West Conshohocken, PA.

ASTM E23-18, 2018. "Standard Test Method for Notched Bar Impact Testing of Metallic Materials". *ASTM International*, West Conshohocken, PA.

Barbosa, V. S., Ruggieri, C., 2018. “Fracture toughness testing using non-standard bend specimens – Part I: Constraint effects and development of test procedure”. *Engineering Fracture Mechanics*, Vol. 195, No. 15, pp. 279–296.

Cravero, S., Ruggieri, C., 2005. “Correlation of fracture behavior in high pressure pipelines with axial flaws using constraint designed test specimens – Part I: Plane-strain analyses”. *Engineering Fracture Mechanics*, Vol. 72, No. 9, pp. 1344-1360.

Dodds, R. H., Anderson, T. L., Kirk, M. T., 1991. “A framework to correlate a/W ratio effects on elastic-plastic fracture toughness Jc”. *International Journal of Fracture*, Vol. 48, No. 1, pp. 1-22.

Dodds, R. H., Shih, F. C., Anderson, T. L., 1993. “Continuum and micromechanics treatment of constraint in fracture”. *International Journal of Fracture*, Vol. 64, No. 2, pp. 101-133.

Ericksonkirk, M. T., Shaikh, A., Ericksonkirk M. A., 2008. “Insights and observations arising from curve-fitting the Charpy V-notch and tensile data contained within the United States’ light water reactor surveillance database”. *In Proceedings of the Pressure Vessels and Piping Conference – PVP 2008*. Chicago, USA.

Mann N. R., Schafer R.E., Singpurwalla N. D., 1974. *Methods for statistical analysis of reliability and life data*. Jonh Wiley & Sons, New York.

McCabe, D. E., Merkle, J. G., Wallin, K., 2005. “An Introduction to the Development and Use of the Master Curve Method”. *ASTM Manual Series*: MNL 27, ASTM International.

Nevalainen, M., Dodds, R. H., 1995. “Numerical Investigation of 3-D constraint effects on brittle fracture in SE(B) and C(T) specimens”. International Journal of Fracture, Vol. 74, No. 2, pp. 131-161.

O’Dowd, N. P. Shih, C. F., 1991. “Family of crack tip-fields characterized by a triaxiality parameter: Part I – structure of fields”. *Journal of the Mechanics and Physics of Solids*, Vol. 39, No. 8, pp. 989-1015.

O’Dowd, N. P. Shih, C. F., 1992. “Family of crack tip-fields characterized by a triaxiality parameter: Part II – fracture applications”. *Journal of the Mechanics and Physics of Solids*, Vol. 40, No. 5, pp. 939-963.

Oldfield, W., 1979. “Fitting curves to toughness data”. *Journal of Testing and Evaluation*, Vol. 7, No. 6, pp. 326-333.

Rice, J. R., 1967. “Mechanics of crack tip deformation and extension by fatigue”. In: Grosskreutz, J. C. (Ed*.). Fatigue crack propagation. ASTM STP 415*. Philadelphia: ASTM International, pp. 247-309.

Ruggieri, C., 2011. “Fractus 2D: numerical computation of fracture mechanics parameters for 2-D cracked solids”. *Tech. Rep.: Fractus 2D Software, NAMEF/PNV/USP*, São Paulo.

Wallin, K., 1991. Fracture toughness transition curve shape for ferritic structural steels, in *“Joint FEFG/IICF International Conference on Fracture of Engineering Materials and Structures”*. In: Teoh, S. H., Lee, K. H. (Eds.), Singapore, 83–88.

10. RESPONSIBILITY NOTICE

The authors are the only responsible for the printed material included in this paper.